International Journal of Minerals, Metallurgy and Materials
Volume 24, Number 7, July 2017, Page 745
DOI: 10.1007/s12613-017-1458-6

Combustion characteristics and kinetics of anthracite with added chlorine

Cui Wang[1,2], *Jian-liang Zhang*[1,2], *Guang-wei Wang*[1], *Ke-xin Jiao*[1], *Zheng-jian Liu*[1], *and Kuo-chih Chou*[2]

1) School of Metallurgical and Ecological Engineering, University of Science and Technology Beijing, Beijing 100083, China

2) State Key Laboratory of Advanced Metallurgy, University of Science and Technology Beijing, Beijing 100083, China

(Received: 11 October 2016; revised: 21 February 2017; accepted: 23 February 2017)

Abstract: The combustion process of Yangquan anthracite (YQ) with the addition of 0.045wt%, 0.211wt%, 1.026wt%, and 2.982wt% chlorine was investigated using a thermogravimetric method from an ambient temperature to 1173 K in an air atmosphere. Results show that the YQ combustion characteristics are not significantly affected by an increase in chlorine content. Data acquired for combustion conversion are then further processed for kinetic analysis. Average apparent activation energies determined using the model-free method (specifically the KAS method) are 103.025, 110.250, 99.906, and 110.641 kJ/mol, respectively, and the optimal kinetic model for describing the combustion process of chlorine-containing YQ is the nucleation kinetic model, as determined by the $z(\alpha)$ master plot method. The mechanism function of the nucleation kinetic model is then employed to estimate the pre-exponential factor, by making use of the compensation effect. The kinetic models to describe chlorine-containing YQ combustion are thus obtained through advanced determination of the optimal mechanism function, average apparent activation energy, and the pre-exponential factor.

Keywords: chlorine; anthracite; combustion characteristics; kinetics

1. Introduction

With rapid global population growth and associated environmental pollution, there is a rising demand for water and a danger of over-exploiting fresh water resources. In response to the national requirements of many countries to save water, the blast furnace (BF) dry-dedusting system has been widely introduced into iron-making plants. However, the released HCl and other acid gases, which should have been absorbed by gas washing water in the BF wet-dedusting system, cause damage to gas pipelines, BF top gas recovery turbine unit, etc. [1–4]. In addition, an increase in chlorine has adverse effects on the BF smelting process, the metallurgical properties of raw materials and coke, the characteristics of molten slag [5–7], and the combustion characteristics of pulverized coal [8]; the circulation and accumulation of chlorine in BF makes these effects more obvious [9–10].

Chlorine exists in BFs in relation to iron ores, coke, and pulverized coal [3]. There has recently been an increase in the injection rate of pulverized coal into BFs, and low-quality coal is extensively utilized for injection [11–12]. It is therefore urgently necessary to clarify the behavior and influence of chlorine on the combustion characteristics of coal injected into BFs under this regime. When Hu *et al.* [8] investigated the effect of chlorine on the combustion process of pulverized coal in the tuyere zone, it was found that the influence of chlorine depends on its existence form within the coal. If chlorine exists as chlorides, such as NaCl, KCl, and $CaCl_2$, the combustion process of the pulverized coal is prevented. In contrast, the combustion process is improved if chorine is combined with HCl and nitrogen functional groups of coal macromolecules [8]. However, the basic influence of chlorine on coal combustion characteristics has not been reported; in particular, the combustion process parameters have not yet been referred to, such as the initial reaction temperature, final reaction temperature, and maximum combustion rate, which play a considerable role in measuring the coal combustion performance. It is thus imperative to study the fundamental influence of chlorine on the combustion process of coal at low temperatures, to better understand the influence of chlorine on the combustion performance of coal in a BF tuyere raceway at high temperatures.

It is generally known that pulverized coal injected into a BF tuyere raceway commonly consists of anthracite and bi-

Corresponding author: Jian-liang Zhang E-mail: zhang.jianliang@hotmail.com

tuminous coal, and that anthracite usually accounts for a large proportion. In this study, therefore, the combustion characteristics and kinetics of a type of anthracite were studied systematically to clarify the fundamental influence of chlorine on the anthracite combustion process.

2. Experimental

2.1. Sample preparation

Yangquan anthracite (YQ) is popularly applied to BF production in China and is thus adopted in the present study, and the properties of YQ are listed in Tables 1 and 2. The sample was dried in a drying oven at 105°C for 24 h and then grinded and sieved to particle sizes less than 0.074 mm. Reagent-grade chemical $CaCl_2$, which had been previously processed by a ball grinder to less than 0.074 mm, was then prepared to adjust the chlorine content in YQ; The contents of chlorine were adjusted to 0.045wt%, 0.211wt%, 1.026wt%, and 2.982wt%. To confirm the role that Ca plays in YQ combustion, 2.433wt% reagent-grade chemical CaO was added to YQ to enable a comparative study, in which the content of Ca was the same as that of YQ with the addition of 2.982wt% chlorine. Certainly, the existence of Ca is important in the combustion process, while the CaO content in raw YQ is 0.288wt%, which is nearly negligible compared with the additive of 2.433wt% CaO. All mixtures were blended in an agate mortar for 30 min to homogenize completely and then stored hermetically for subsequent experiments.

Table 1. Proximate and ultimate analysis of YQ

Proximate analysis / wt%				Ultimate analysis / wt%					ω(Cl) / wt%
FC_d	A_d	V_d	M_{ad}	C_d	H_d	O_d	N_d	S_d	
70.50	17.06	11.60	0.84	72.39	4.08	13.32	1.25	0.18	0.045

Note: FC—fixed carbon; A—ash; V—volatile; M—moisture; d—dry basis; ad—air dried basis.

Table 2. Ash composition of YQ wt%

CaO	SiO_2	Al_2O_3	MgO	Fe_2O_3	K_2O	Na_2O	P_2O_5	SO_3
1.69	54.52	36.04	0.49	2.25	0.34	0.48	0.29	2.15

2.2. Experimental apparatus and procedure

The experiments were performed using a thermogravimetric analyzer (WCT-2C, Beijing Optical Instrument Factory) at atmospheric pressure. To minimize the effects caused by mass and heat transfer limitation, a small amount of each sample (5 mg) was loaded into an Al_2O_3 crucible (ϕ5 mm × 2 mm) for each run, and all samples were heated up under a continuous gas flow of 60 mL/min compressed air from ambient temperature to 900°C and maintained for 15 min to enable complete combustion. Corresponding thermogravimetry (TG) and differential thermogravimetry (DTG) combustion curves were obtained at heating rates of 5, 10, and 20 K/min [13–14], and certain crucial experiments were repeated twice to ensure reproducibility of results.

The combustion conversion, α, was calculated using the following equation:

$$\alpha=\frac{m_0-m_t}{m_0-m_\infty} \tag{1}$$

where m_0 represents the initial mass, m_t is the instantaneous mass at time t, and m_∞ is the remaining mass of coal after complete combustion.

2.3. Characterization of coal combustion

The TG–DTG method [15] was adopted to enable quantitative analysis of the characterization of chlorine-containing YQ combustion, and the initial combustion temperature (T_i), total combustion temperature (T_f), and combustion time (t_g) are obtainable from TG–DTG curves. The parameter, T_i, is evaluated for different samples to compare their activities in the same reaction-off process or under the same operating conditions: it is not a physical property of the fuel. T_f denotes the temperature at a mass loss of above 95%. The comprehensive combustion characteristic index, S, is defined as follows [16]:

$$S=\frac{(\mathrm{d}\omega/\mathrm{d}t)_{\max}(\mathrm{d}\omega/\mathrm{d}t)_{\mathrm{mean}}}{T_i^2T_f} \tag{2}$$

where $\mathrm{d}\omega/\mathrm{d}t$ represents the mass loss rate (wt%/min), $(\mathrm{d}\omega/\mathrm{d}t)_{\max}$ is the maximum combustion rate (wt%/min), and $(\mathrm{d}\omega/\mathrm{d}t)_{\mathrm{mean}}$ is the mean combustion rate (wt%/min).

3. Results and discussion

3.1. Thermogravimetric analysis

Fig. 1 shows the influence of CaO on YQ combustion; it can be observed that the conversion curve of YQ combustion shifts to a lower temperature zone with the addition of CaO. It can thus be generally concluded that CaO promotes YQ combustion.

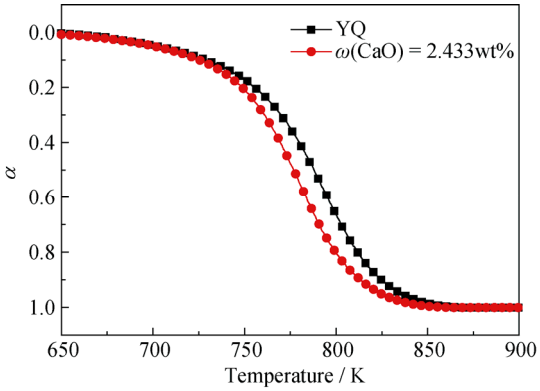

Fig. 1. Conversion curve of YQ combustion with 2.433wt% CaO.

The conversion and conversion rate results of YQ are shown in Fig. 2. As all conversion rate curves have only one peak, the YQ combustion process can be commonly divided into three stages as follows: (1) Stage one, mass decreases slightly due to the volatilization of water and a little volatile within the temperature range of ambient temperature to T_i; (2) Stage two, mass decreases rapidly due to the fierce combustion of coal particles within the temperature range of T_i to T_f; (3) Stage three, mass remains constant due to complete combustion of the coal sample and ash remaining within a temperature higher than T_f. Combustion mainly happens in the second stage and therefore the kinetic analysis is primarily concentrated on this stage.

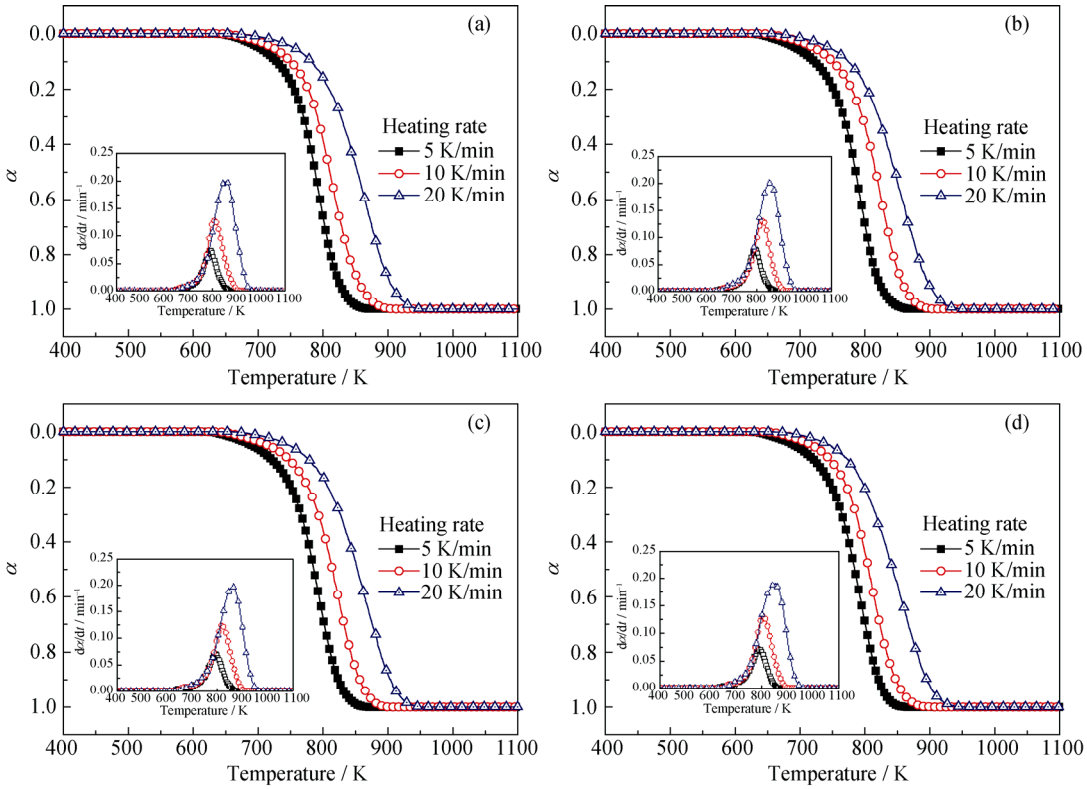

Fig. 2. Conversion and conversion rate curves of YQ with different chlorine contents: (a) 0.045wt%; (b) 0.211wt%; (c) 1.026wt%; (d) 2.982wt%.

From Fig. 2, it is also evident that the conversion curves are similar to each other at different heating rates and that they move to the higher temperature zone with an increase in heating rate. In this respect, increasing the heating rate results in a faster increase in temperature and there is not enough time for parts of the reactions to be completed or to achieve a balance. In addition, there is a hysteresis for temperature increasing as the heating rate increases, which also leads to combustion in a higher temperature zone.

Table 3 shows the characteristic combustion parameters of YQ at different heating rates. Theoretically, coal ignition undergoes a state transformation from slow oxidation to fierce combustion, and T_i reflects the difficulty involved in coal ignition. T_f represents the temperature at which the fixed carbon and volatiles are burned out; a lower value of T_f indicates a shorter burnout time and fewer combustible materials remaining in the carbon residue. Generally, lower values of T_i and T_f indicate that a higher degree of combustion reaction has occurred; however, as T_i and T_f cannot completely embody coal combustion characteristics, the comprehensive combustion characteristic index, S, is employed instead where a larger S value indicates better combustion characteristics.

Table 3. Characteristic combustion parameters of YQ at different heating rates

ω(Cl) / wt%	β / (K·min^{-1})	T_i / °C	T_f / °C	$(d\omega/dt)_{max}$ / (wt%·min^{-1})	$(d\omega/dt)_{mean}$ / (wt%·min^{-1})	t_g / min	S / 10^{-7}
0.045	5	487.0	595.4	6.58	3.32	20.10	1.55
	10	498.2	628.1	10.89	5.85	11.77	4.09
	20	528.6	673.8	18.20	11.31	6.58	10.93
0.211	5	481.8	592.3	7.36	3.53	20.22	1.89
	10	503.6	626.1	11.97	6.45	11.28	4.86
	20	522.9	669.9	18.50	10.90	6.72	11.01
1.026	5	480.6	589.2	6.47	3.52	20.02	1.67
	10	490.6	626.5	11.21	6.03	12.53	4.48
	20	526.7	681.5	18.03	10.21	7.20	9.74
2.982	5	477.1	585.1	5.98	3.30	19.62	1.48
	10	495.0	618.7	10.86	5.79	11.43	4.15
	20	517.9	670.3	16.40	9.97	6.98	9.09

Table 3 also shows the decrease trend of T_i, T_f, $(d\omega/dt)_{max}$, and $(d\omega/dt)_{mean}$ of YQ combustion with an increase in chlorine content; however, this occurs within a small declining range. When the chlorine content of YQ is increased from 0wt% to 2.982wt%, T_i decreases from 487.0, 498.2, and 528.6°C to 477.1, 495.0, and 517.9°C, respectively, at the heating rates of 5, 10, and 20 K/min; and T_f respectively decreases from 595.4, 628.1, and 673.8°C to 585.1, 618.7, and 670.3°C. These results indicate that chlorine has a slight effect on the T_i and T_f of YQ. In addition, the low decreasing range of $(d\omega/dt)_{max}$ and $(d\omega/dt)_{mean}$ also indicates that they are slightly affected by the addition of chlorine.

The S value of YQ also shows a decrease trend with an increase in chlorine, but this occurs only to a small extent; this is consistent with the performance of T_i, T_f, $(d\omega/dt)_{max}$ and $(d\omega/dt)_{mean}$. When the chlorine content is increased from 0wt% to 2.982wt%, the S value changes from 1.55×10^{-7}, 4.09×10^{-7}, and 10.93×10^{-7} to 1.48×10^{-7}, 4.15×10^{-7}, and 9.09×10^{-7} at the heating rates of 5, 10, and 20 K/min, respectively. However, the S value increases marginally when the chlorine content is below 0.211wt%, and the same phenomenon occurs with T_i, T_f, $(d\omega/dt)_{max}$, and $(d\omega/dt)_{mean}$; this result may be related to the preponderance of the promoted role of calcium ions in the lower chlorine content.

Based on the above analyses the following can be inferred: an increase in chlorine inhibits the decomposition of combustible materials, decreases the combustion rate, and extends combustion time, thereby causing a final reduction in YQ reactivity. Table 3 also shows that with an increase in heating rate there is an increase in T_i, T_f, $(d\omega/dt)_{max}$, $(d\omega/dt)_{mean}$, and S of YQ, and t_g is shortened correspondingly. It is thus evident that YQ reactivity can be improved by increasing the heating rate.

3.2. Kinetic analysis

3.2.1. Determination of apparent activation energy

The combustion of coal is a gas−solid heterogeneous oxidation reaction, and the reaction rate can be expressed in terms of three major variables: temperature, T; conversion, α; and pressure, P, as follows:

$$\frac{d\alpha}{dt} = k(T)f(\alpha)h(P) \tag{3}$$

where the reaction rate constant, $k(T)$, represents the dependence of the reaction rate on temperature; the ideal reaction model, $f(\alpha)$, depends on the conversion of α; and $h(P)$ is dependent on pressure. Experiments were conducted at atmospheric pressure, and it is thus assumed that the reaction rate is independent of pressure and is described as

$$\frac{d\alpha}{dt} = k(T)f(\alpha) \tag{4}$$

Most kinetic models fundamentally follow the universal Arrhenius law, so the temperature dependence of the reaction rate can be typically parameterized through the Arrhenius equation:

$$k(T) = A\exp\left(-\frac{E}{RT}\right) \tag{5}$$

where E is the apparent activation energy, A is the pre-exponential factor, and R is the universal gas constant.

In the non-isothermal experimental condition, the linearly controlled heating rate, β, is expressed as

$$\beta = \frac{dT}{dt} \tag{6}$$

Substituting Eqs. (5) and (6) into Eq. (4) then yields

$$\frac{\mathrm{d}\alpha}{\mathrm{d}T}=\frac{A}{\beta}\exp\left(-\frac{E}{RT}\right)f(\alpha) \tag{7}$$

and by integrating Eq. (7), the integral form of the reaction model is obtained as

$$g(\alpha)=\int_0^{\alpha}\frac{\mathrm{d}\alpha}{f(\alpha)}=\frac{A}{\beta}\int_0^{T}\exp\left(-\frac{E}{RT}\right)\mathrm{d}T \tag{8}$$

The resulting Eqs. (7) and (8) lay the foundation for the differential and integral kinetic methods used in various kinetic analyses.

The model-free method (isoconversional method) can be applied to evaluate the apparent activation energy without the requirement of identifying any particular form of the reaction model. In accordance with the recommendations developed by the Kinetics Committee of the International Confederation for Thermal Analysis and Calorimetry (ICTAC), experiments of 3–5 runs at different heating rates were carried out to obtain the temperature dependence of the isoconversional rate. The apparent activation energy was determined within a wide range of α = 0.05–0.95 with a step no larger than 0.05. The relative accurate Kissinger-Akahira-Sunose (KAS) equation was then adopted to estimate E_α [17]:

$$\ln\left(\frac{\beta_i}{T_{\alpha,i}^2}\right)=\text{const}-\frac{E_\alpha}{RT_\alpha} \tag{9}$$

where i identifies an individual heating rate, E_α and T_α are the apparent activation energy and temperature at given α, respectively. Therefore, E_α values can be determined from the slope of the linear representation of $\ln(\beta_i / T_{\alpha,i}^2)$ vs. $1/T_\alpha$, as shown in Fig. 3, and the calculation results are shown in Table 4.

The average apparent activation energies of YQ combustion with different chlorine contents calculated by the KAS method are 103.025, 110.250, 99.906, and 110.641 kJ/mol, respectively. Table 4 and Fig. 4 show the small variation in apparent activation energies for each of the different chlorine-containing YQ combustions with the degree of conversion. This indicates that a single-step reaction occurs during chlorine-containing YQ combustions. In addition, Fig. 4 shows that the apparent activation energy firstly increases and then decreases, which illustrates the relationship between the apparent activation energy and the conversion. The reason for this phenomenon may come from the initial volatilization of water and a little volatile occurred during the first stage. The increase in apparent activation energy at a low conversion interval can be explained by a decrease in the active functional groups and surface moisture of YQ during the volatilization process. When the volatilization reaction reaches a certain extent, the volatiles released ignite and burn. The formation of a porous structure promotes faster gaseous diffusion and leads to a decrease in activation energy.

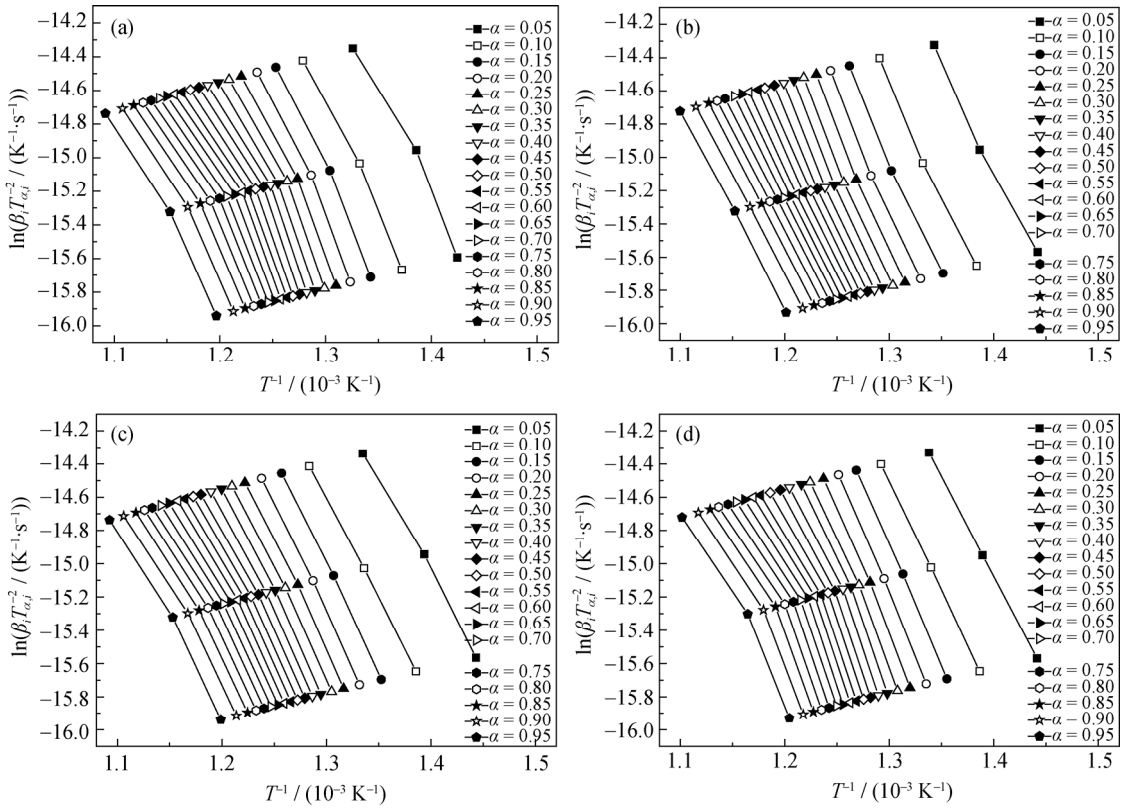

Fig. 3. KAS plots of YQ with different chlorine contents: (a) 0.045wt%; (b) 0.211wt%; (c) 1.026wt%; (d) 2.982wt%.

Table 4. Apparent activation energies of YQ with different chlorine contents obtained using the KAS method

α	ω(Cl) / wt%							
	0.045		0.211		1.026		2.982	
	E / (kJ·mol^{-1})	R^2	E / (kJ·mol^{-1})	R^2	E / (kJ·mol^{-1})	R^2	E / (kJ·mol^{-1})	R^2
0.05	102.761	0.9620	103.927	0.9892	93.877	0.9935	99.459	1.0000
0.10	109.830	0.9826	111.196	0.9906	100.424	0.9993	109.544	0.9997
0.15	114.988	0.9834	115.594	0.9913	107.948	0.9984	120.189	0.9992
0.20	116.758	0.9787	120.432	0.9917	109.944	0.9976	124.396	0.9986
0.25	114.005	0.9708	122.358	0.9920	108.691	0.9952	125.997	0.9949
0.30	112.589	0.9601	121.501	0.9920	107.425	0.9956	123.943	0.9881
0.35	110.633	0.9548	122.217	0.9935	107.883	0.9941	125.807	0.9806
0.40	106.712	0.9396	118.986	0.9933	104.887	0.9929	120.221	0.9656
0.45	104.534	0.9334	115.623	0.9951	102.011	0.9897	118.111	0.9637
0.50	102.436	0.9378	112.264	0.9987	101.388	0.9897	113.005	0.9521
0.55	99.726	0.9392	111.628	0.9972	99.549	0.9869	109.480	0.9434
0.60	97.955	0.9328	107.811	0.9984	98.940	0.9863	107.880	0.9386
0.65	96.954	0.9423	106.760	0.9995	96.187	0.9848	105.346	0.9301
0.70	96.040	0.9513	104.489	0.9997	94.885	0.9835	103.178	0.9327
0.75	94.562	0.9503	101.265	1.0000	93.069	0.9799	101.870	0.9268
0.80	94.446	0.9589	100.536	1.0000	93.135	0.9827	99.760	0.9309
0.85	93.830	0.9661	100.446	1.0000	93.051	0.9841	99.792	0.9389
0.90	94.436	0.9719	98.658	0.9998	91.857	0.9822	98.276	0.9495
0.95	94.283	0.9752	99.054	0.9988	93.056	0.9827	95.930	0.9548
Average	103.025		110.250		99.906		110.641	

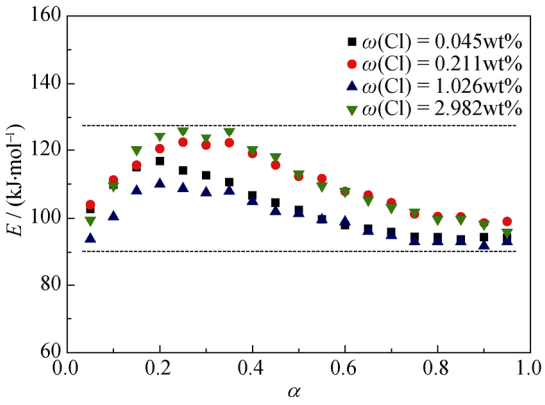

Fig. 4. Variation in apparent activation energy of YQ with different chlorine contents with conversion.

3.2.2. Determination of reaction model

The dependence of the YQ combustion conversion rate on conversion at different heating rates is shown in Fig. 5. The conversion rate firstly increases to a peak value and then decreases along with an increase in conversion. This is related to the following: at an early stage of combustion the increasing temperature promotes the increase of the conversion rate, but only to a certain degree. The reduction in specific surface area and active particles leads to a decrease in conversion rate, although the temperature continues to rise [18]. The increased heating rate also leads to a systematically increased conversion rate, while the maximum conversion rate appears at an approximately constant conversion of 0.55, independent of the heating rate. This implies that the fundamental combustion mechanism is only minimally affected by the heating rate [19].

The ideal reaction model, $f(\alpha)$, represents the dependence of the reaction rate on conversion, α, some of the kinetic models used in solid-state kinetics are listed in Table 5 [20−21]. To determine the most appropriate kinetic model to describe the chlorine-containing YQ combustions, Eq. (5) is substituted into Eq. (4) and rearranged to obtain the $y(\alpha)$ master plot in the following expression:

$$y(\alpha)=\left(\frac{\mathrm{d}\alpha}{\mathrm{d}t}\right)_{\alpha}\exp\left(\frac{E_0}{RT_{\alpha}}\right)=Af(\alpha) \tag{10}$$

where $(\mathrm{d}\alpha/\mathrm{d}t)_{\alpha}$ is the reaction rate at a given conversion α and heating rate β, and E_0 is the average value of E_{α} calculated using the KAS method.

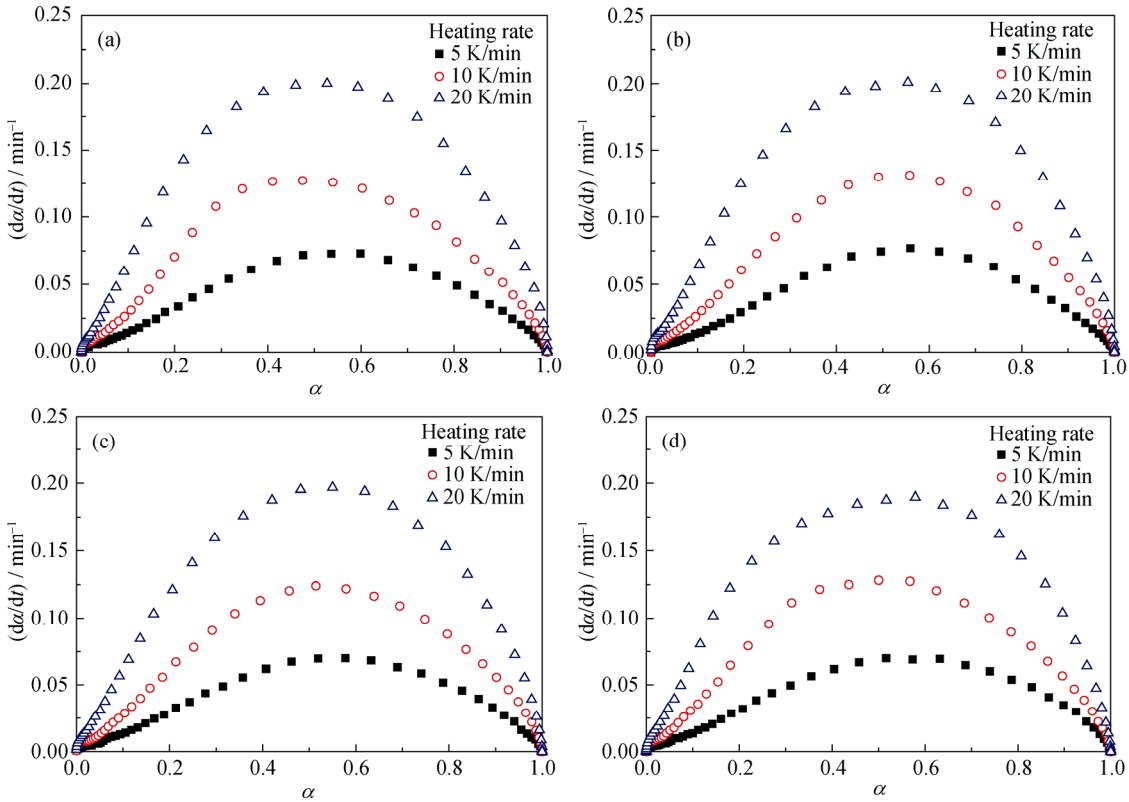

Fig. 5. Experimental conversion rate as a function of conversion for combustion of YQ with different chlorine contents: (a) 0.045wt%; (b) 0.211wt%; (c) 1.026wt%; (d) 2.982wt%.

Table 5. Differential and integral forms of kinetic models used in solid-state kinetics

Reaction model		Code	$f(\alpha)$	$g(\alpha)$
Reaction order	First-order	F1	$1-\alpha$	$-\ln(1-\alpha)$
	Second-order	F2	$(1-\alpha)^2$	$(1-\alpha)^{-1}-1$
	Third-order	F3	$(1-\alpha)^3$	$[(1-\alpha)^{-2}-1]/2$
Power law	Power law	P23	$(2/3)\alpha^{-1/2}$	$\alpha^{3/2}$
	Power law	P2	$2\alpha^{1/2}$	$\alpha^{1/2}$
	Power law	P3	$3\alpha^{2/3}$	$\alpha^{1/3}$
	Power law	P4	$4\alpha^{3/4}$	$\alpha^{1/4}$
Diffusion	One-dimensional diffusion	D1	$(1/2)\alpha^{-1}$	α^2
	Two-dimensional diffusion	D2	$[-\ln(1-\alpha)]^{-1}$	$\alpha+(1-\alpha)\ln(1-\alpha)$
	Three-dimensional diffusion	D3	$[(3/2)(1-\alpha)^{2/3}]/[1-(1-\alpha)^{1/3}]$	$[1-(1-\alpha)^{1/3}]^2$
	Ginstling-Brounshtein	D4	$[(3/2)(1-\alpha)^{1/3}]/[1-(1-\alpha)^{1/3}]$	$(1-2\alpha/3)-(1-\alpha)^{2/3}$
Nucleation	Avrami-Erofeev	A15	$1.5(1-\alpha)[-\ln(1-\alpha)]^{1/3}$	$[-\ln(1-\alpha)]^{2/3}$
	Avrami-Erofeev	A2	$2(1-\alpha)[-\ln(1-\alpha)]^{1/2}$	$[-\ln(1-\alpha)]^{1/2}$
	Avrami-Erofeev	A3	$3(1-\alpha)[-\ln(1-\alpha)]^{2/3}$	$[-\ln(1-\alpha)]^{1/3}$
	Avrami-Erofeev	A4	$4(1-\alpha)[-\ln(1-\alpha)]^{3/4}$	$[-\ln(1-\alpha)]^{1/4}$
Geometrical contraction	Contracting sphere	R2	$2(1-\alpha)^{1/2}$	$1-(1-\alpha)^{1/3}$
	Contracting cylinder	R3	$3(1-\alpha)^{2/3}$	$1-(1-\alpha)^{1/2}$

The $z(\alpha)$ master plot is introduced as

$$z(\alpha) = f(\alpha)g(\alpha) = \left(\frac{\mathrm{d}\alpha}{\mathrm{d}t}\right)_{\alpha} T_{\alpha}^{2}\left[\frac{\pi(x)}{\beta T_{\alpha}}\right] \quad (11)$$

where $x = E_{\alpha}/RT$, $\pi(x)$ is an approximation of the temperature integral, and the fourth rational approximation performed by Senum and Yang [22] is given as

$$\pi(x) = \frac{x^3 + 18x^2 + 88x + 96}{x^4 + 20x^3 + 120x^2 + 240x + 120} \quad (12)$$

The $y(\alpha)$ and/or $z(\alpha)$ values calculated directly from experimental data are consequently plotted as a function of α and are compared against theoretical $y(\alpha)$ and/or $z(\alpha)$ master plots to determine the most appropriate kinetic model. However, the constant, A, is yet unknown, and the experimental and theoretical $y(\alpha)$ master plots need to be normalized so that they vary from 0 to 1 in the same manner. In the present study, normalization of experimental and theoretical $y(\alpha)$ is performed using the following equation:

$$y(\alpha)_{\mathrm{norm}} = \frac{y(\alpha)}{\max[y(\alpha)]} \quad (13)$$

Fig. 6 shows the theoretical normalized $y(\alpha)$ and actual $z(\alpha)$ master plots for the kinetic models shown in Table 5. A comparison with the experimental $z(\alpha)$ master plots from Fig. 7 shows that the most probable kinetic models used to describe the chlorine-containing YQ combustion are those

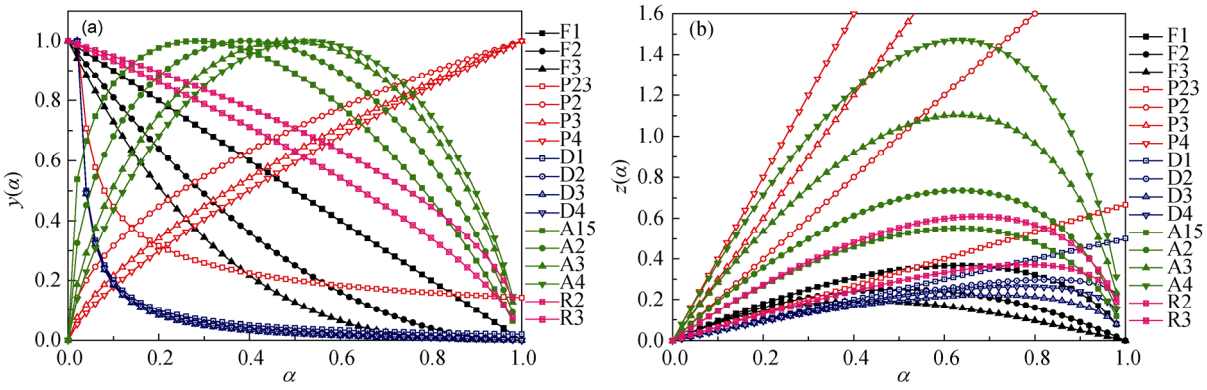

Fig. 6. Theoretical normalized $y(\alpha)$ and actual $z(\alpha)$ master plots for kinetic models shown in Table 5: (a) $y(\alpha)$; (b) $z(\alpha)$.

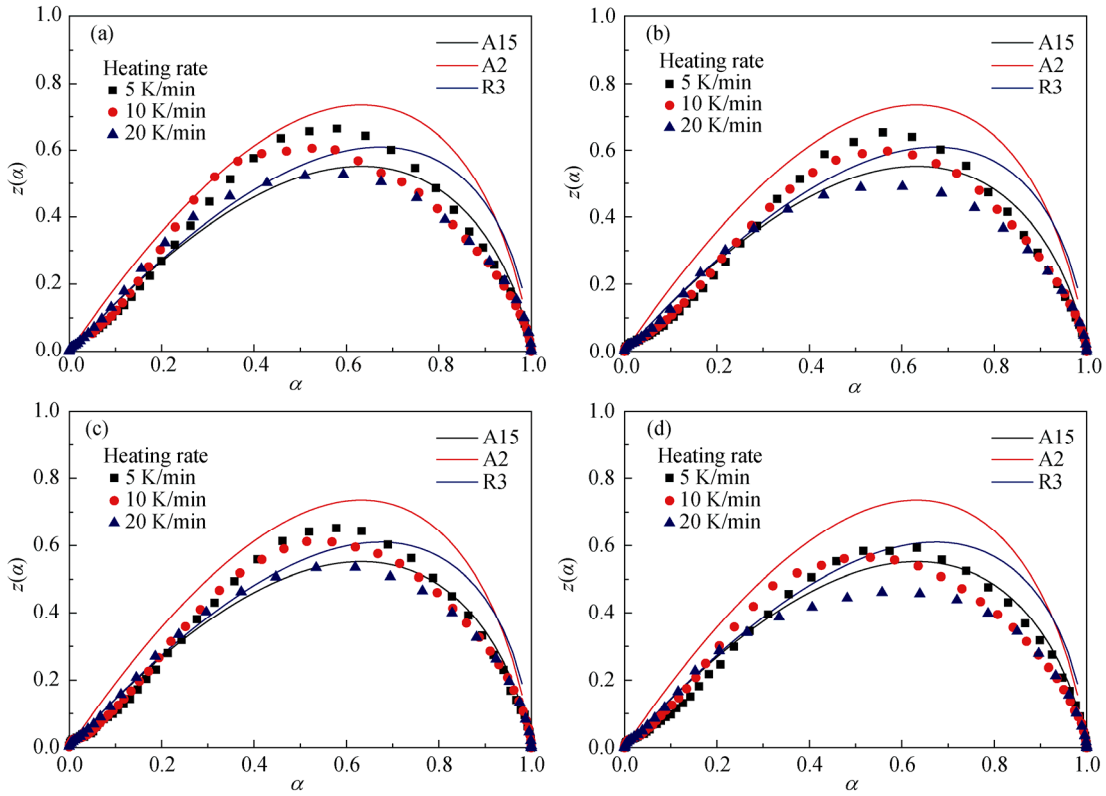

Fig. 7. Experimental $z(\alpha)$ master plots for combustion of YQ with different chlorine contents: (a) 0.045wt%; (b) 0.211wt%; (c) 1.026wt%; (d) 2.982wt%.

of A15, A2, and R3. Therefore, the A15, A2, and R3 profiles are also plotted in Fig. 7 to ascertain the optimal kinetic model. It can be observed from Fig. 7 that the chlorine-containing YQ combustion matches well using the A15 theoretical kinetic model, especially at higher conversions and in higher chlorine contents. Therefore, the mechanism function of the A15 kinetic model is employed to determine the pre-exponential factor.

3.2.3. Determination of pre-exponential factor

The method of invariant kinetic parameters [23], which makes use of the so-called "compensation effect", is adopted to determine the pre-exponential factor of chlorine-containing YQ combustion. By substituting the mechanism function $f(\alpha)$ values of the A15 kinetic model at different conversions and heating rates into Eq. (7), different pairs of $\ln A_\alpha$ and E_α are obtained. Although the parameters vary widely with different mechanism functions, $f(\alpha)$, they all deonstrate a strong correlation; this is known as the compensation effect,

$$\ln A_\alpha = aE_\alpha + b \tag{14}$$

Parameters a and b are constants and can be calculated from the slope and intercept of the linear fitting of $\ln A_\alpha$ as a function of E_α under the three heating rates. The pre-exponential factor, A_0, can then be determined with the substitution of the average activation energy determined using the model-free method into Eq. (14):

$$\ln A_0 = aE_0 + b \tag{15}$$

Fig. 8 shows the relationship between activation energy and pre-exponential factor at different heating rates, where the natural logarithmic pre-exponential factor is linearly related to the activation energy. This indicates that the kinetic compensation effect does exist in the YQ combustion process, which also proves the applicability of the kinetic model in describing the complicated combustion process involved in anthracite with added chlorine. The parameters a and b obtained from linear fitting are listed in Table 6; the A_0 values of chlorine-containing YQ are calculated as 6.8778×10^5, 2.0664×10^6, 4.1462×10^5, and 2.4022×10^6 min^{-1}, respectively. Therefore, kinetic models for different chlorine-containing YQ combustion can be obtained through the optimal mechanism function, the average apparent activation energy, and the pre-exponential factor. The kinetic models of YQ combustion with 0.045wt%, 0.211wt%, 1.026wt%, and 2.982wt% chlorine can thus be expressed as

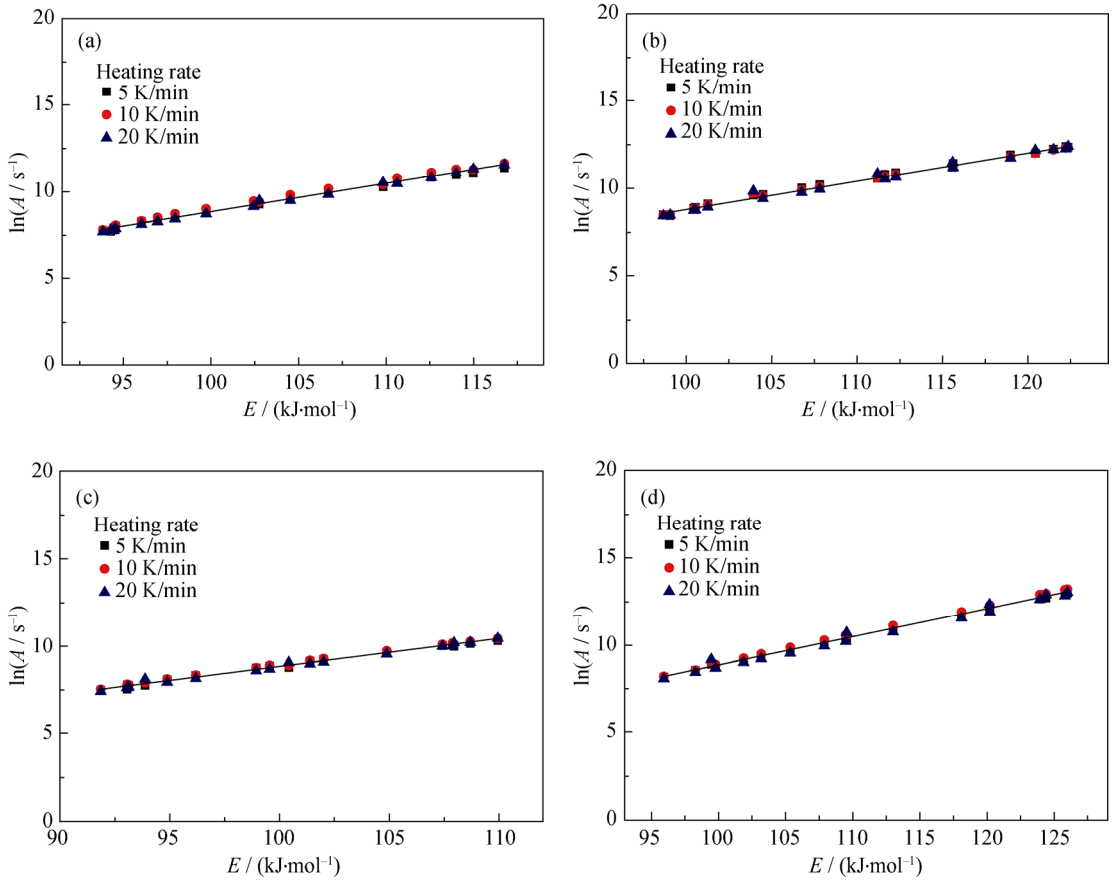

Fig. 8. Compensation effect between activation energy and pre-exponential factor of combustion of YQ with different chlorine contents: (a) 0.045wt%; (b) 0.211wt%; (c) 1.026wt%; (d) 2.982wt%.

Table 6. Pre-exponential factors of combustion of YQ with different chlorine contents calculated using the method of invariant kinetic parameters

ω(Cl) / wt%	a	b	R^2	E_0 / (kJ·mol^{-1})	A_0 / min^{-1}
0.045	1.6311×10^{-4}	–7.4570	0.9899	103.025	6.8778×10^5
0.211	1.6150×10^{-4}	–7.3582	0.9919	110.250	2.0664×10^6
1.026	1.6038×10^{-4}	–7.1825	0.9914	99.906	4.1462×10^5
2.982	1.6206×10^{-4}	–7.3327	0.9923	110.641	2.4022×10^6

$$\frac{d\alpha}{dt} = 1.0317\times10^6 \exp\left(-\frac{103025}{RT}\right)(1-\alpha)[-\ln(1-\alpha)]^{1/3} \quad (16)$$

$$\frac{d\alpha}{dt} = 3.0996\times10^6 \exp\left(-\frac{110250}{RT}\right)(1-\alpha)[-\ln(1-\alpha)]^{1/3} \quad (17)$$

$$\frac{d\alpha}{dt} = 6.2193\times10^5 \exp\left(-\frac{99906}{RT}\right)(1-\alpha)[-\ln(1-\alpha)]^{1/3} \quad (18)$$

$$\frac{d\alpha}{dt} = 3.6033\times10^6 \exp\left(-\frac{110641}{RT}\right)(1-\alpha)[-\ln(1-\alpha)]^{1/3} \quad (19)$$

4. Conclusions

The combustion characteristics and kinetics of YQ with 0.045wt%, 0.211wt%, 1.026wt%, and 2.982wt% chlorine under non-isothermal conditions were investigated to elucidate the influence of chlorine on anthracite combustion and to ascertain the kinetic behaviors in chlorine-containing YQ combustion. Thermogravimetric analysis revealed that YQ combustion is slightly affected by the addition of chlorine, and combustion reactivity can be improved by increasing the heating rate. In addition, the model-free method was employed to evaluate the average apparent activation energy, and the values calculated by the KAS method were 103.025, 110.250, 99.906, and 110.641 kJ/mol, respectively. A comparison between the experimental and theoretical $z(\alpha)$ master plots indicated that A15 is the optimal kinetic model for use in describing the combustion process of YQ with the addtion of chlorine; thus the mechanism function of the A15 kinetic model was adopted to determine the pre-exponential factor. The values determined by the method of invariant kinetic parameters are 6.8778×10^5, 2.0664×10^6, 4.1462×10^5, and 2.4022×10^6 min^{-1}, respectively. Furthermore, kinetic models used to describe chlorine-containing YQ combustion were obtained through the advanced determination of the optimal mechanism function, the average apparent activation energy, and the pre-exponential factor.

Acknowledgements

This work was financially supported by the Beijing Municipal Science & Technology Commission of China (No. Z161100002716017), the Key Program of the National Natural Science Foundation of China (No. U1260202), and the 111 Project (No. B13004).

References

[1] M. Okeda, M. Hasegawa, and M. Iwase, Solubilities of chlorine in CaO–SiO_2–Al_2O_3–MgO slags: correlation between sulfide and chloride capacities, *Metall. Mater. Trans. B*, 42(2011), No. 2, p. 281.

[2] B.S. Hu, Y.L. Gui, H.L. Guo, and C.Y. Song, Behaviors of chlorine in smelting process of blast furnace, *Adv. Mater. Res.*, 396-398(2012), p. 152.

[3] E. Lectard, E. Hess, and R. Lin, Behaviour of chlorine and alkalis in the blast furnace and effect on sinter properties during reduction, *Rev. Met. Paris*, 101(2004), No. 1, p. 31.

[4] X.J. Liu, Q. Lü, and S.H. Zhang, Migration principle of chlorine in BF production, *Adv. Mater. Res.*, 402(2012), p. 107.

[5] H.M. Yang, G.Z. Qiu, and A.D. Tang, Effect of $CaCl_2$ on sinter RDI, *J. Cent. South Univ. Technol.*, 29(1998), No. 3, p. 28.

[6] Z.Y. Wang, X.L. Wang, D.J. Liu, W. Zhang, N. Zhang, and B. Hao, Effect of $CaCl_2$ on alkali metal enrichment and thermal performance of coke in blast furnace, *Ironmaking*, 28(2009), No. 3, p. 45.

[7] B.S. Hu, Y.L. Gui, X.G. Han, and H.L. Guo, Influence of HCl in gas on the metallurgical property of material and fuel used in blast furnace, *China Metall.*, 21(2011), No. 10, p. 15.

[8] B.S. Hu, Y.L. Gui, H.L. Guo, and C.Y. Song, Effect of chlorine on combustion process of pulverized coal in tuyere zone, *Adv. Mater. Res.*, 291-294(2011), p. 1203.

[9] E. Jak and P. Hayes, The use of thermodynamic modeling to examine alkali recirculation in the iron blast furnace, *High Temp. Mater. Processes*, 31(2012), No. 4-5, p. 657.

[10] Y.Y. Yang and Z.K. Gao, Study on the mechanism of scaffolding caused by alkali cycling and accumulation and promoted by the presence of fluorine in the blast furnaces of Baotou Iron and Steel Co. and measures to prevent scabfomation, *Iron Steel*, 18(1983), No. 12, p. 32.

[11] Y. Ogaki, K. Tomioka, A. Watanabe, K. Arita, I. Kuriyama, and T. Sugayoshi, Recycling of waste plastic packaging in a blast furnace system, *NKK Tech. Rev.*, (2001), No. 84, p. 1.

[12] K.J. Myoung, Y.S. Lee, D.J. Min, U.C. Chung, and S.H. Yi, Thermodynamic behaviour of chlorine in CaO–SiO_2–MgO–Al_2O_3(–CaF_2) slags, *Steel Res. Int.*, 75(2004), No. 12, p. 783.

[13] J.L. Zhang, J. Guo, G.W. Wang, T. Xu, Y.F. Chai, C.L. Zheng, and R.S. Xu, Kinetics of petroleum coke/biomass blends during co-gasification, *Int. J. Miner. Metall. Mater.*, 23(2016), No. 9, p. 1001.

[14] H.M. Shao, X.Y. Shen, Y. Sun, Y. Liu, and Y.C. Zhai, Reaction condition optimization and kinetic investigation of roasting zinc oxide ore using $(NH_4)_2SO_4$, *Int. J. Miner. Metall. Mater.*, 23(2016), No. 10, p. 1133.

[15] Y.G. Xu, C. Zhang, J. Xia, Y.H. Duan, J.J. Yin, and G. Chen, Experimental study on the comprehensive behavior of combustion for blended coals, *Asia-Pac. J. Chem. Eng.*, 5(2010), No. 3, p. 435.

[16] X.G. Li, Y. Lv, B.G. Ma, S.W. Jian, and H.B. Tan, Thermogravimetric investigation on co-combustion characteristics of tobacco residue and high-ash anthracite coal, *Bioresour. Technol.*, 102(2011), No. 20, p. 9783.

[17] T. Akahira and T. Sunose, Method of determining activation deterioration constant of electrical insulating materials, *Res. Rep. Chiba Inst. Technol. Sci. Technol.*, 16(1971), p. 22.

[18] Y. Sekine, K. Ishikawa, E. Kikuchi, M. Matsukata, and A. Akimoto, Reactivity and structural change of coal char during steam gasification, *Fuel*, 85(2006), No. 2, p. 122.

[19] X.Y. Zheng, D.K. Li, C.Y. Feng, and X.T. Chen, Thermal properties and non-isothermal curing kinetics of carbon nanotubes/ionic liquid/epoxy resin systems, *Thermochim. Acta*, 618(2015), p. 18.

[20] S. Vyazovkin, A.K. Burnham, J.M. Criado, L.A. Pérez-Maqueda, C. Popescu, and N. Sbirrazzuoli, ICTAC Kinetics Committee recommendations for performing kinetic computations on thermal analysis data, *Thermochim. Acta*, 520(2011), No. 1-2, p. 1.

[21] D. Kumar, S.C. Maiti, and C. Ghoroi, Decomposition kinetics of $CaCO_3$ dry coated with nano-silica, *Thermochim. Acta*, 624(2016), p. 35.

[22] G.I. Senum and R.T. Yang, Rational approximations of the integral of the Arrhenius function, *J. Therm. Anal.*, 11(1977), No. 3, p. 445.

[23] A.I. Lesnikovich and S.V. Levchik, A method of finding invariant values of kinetic parameters, *J. Therm. Anal.*, 27(1983), No. 1, p. 89.